JOURNAL OF QUATERNARY SCIENCE (2019) 1–17 ISSN 0267-8179. DOI: 10.1002/jqs.3138

JQS Journal of Quaternary Science QRA Quaternary Research Association

Refining the ice flow chronology and subglacial dynamics across the migrating Labrador Divide of the Laurentide Ice Sheet with age constraints on deglaciation

JESSEY M. RICE,[1]* MARTIN ROSS,[1] ROGER C. PAULEN,[2] SAMUEL E. KELLEY,[1,6] JASON P. BRINER,[3] CHRISTINA M. NEUDORF[4] and OLAV B. LIAN[5]

[1]Earth and Environmental Sciences, University of Waterloo, Waterloo, ON, Canada
[2]Geological Survey of Canada, Ottawa, ON, Canada
[3]Department of Geology, University at Buffalo, Buffalo, NY, USA
[4]Desert Research Institute, Reno, NV, USA
[5]Department of Geography and the Environment, University of the Fraser Valley, Abbotsford, BC, Canada
[6]School of Earth Science, University College Dublin, Dublin, Ireland

ABSTRACT: The Laurentide Ice Sheet was characterized by a dynamic polythermal base. However, important data and knowledge gaps have led to contrasting reconstructions in areas such as the Labrador Ice Divide. In this study, detailed fieldwork was conducted at the southeastern edge of a major landform boundary to resolve the relative ice flow chronology and constrain the evolution of the subglacial dynamics, including the migration and collapse of the Labrador Ice Divide. Surficial mapping and analysis of 94 outcrop-scale ice flow indicators were used to develop a relative ice flow chronology. ^{10}Be exposure ages were used with optical ages to confine the timing of deglaciation within the study area. Four phases of ice flow were identified. Flow 1 was a northeasterly ice flow preserved under non-erosive subglacial conditions associated with the development of an ice divide. Flow 2 was a northwest ice flow, which we correlate to the Ungava Bay Ice Stream and led to a westward migration of the ice divide, preserving Flow 2 features and resulting in Flow 3's eastward-trending indicators. Flow 4 is limited to sparse fine striations within and around the regional uplands. The new optical ages and ^{10}Be exposure ages add to the regional geochronology dataset, which further constrains the timing of ice margin retreat in the area to around 8.0 ka. Copyright © 2019 The Authors. *Journal of Quaternary Science* Published by John Wiley & Sons Ltd.

KEYWORDS: deglaciation; ice flow chronology; Laurentide Ice Sheet (LIS); Quebec–Labrador Dome.

Introduction

Reconstructing past ice sheets, including their thickness, the extent of land they covered at different times, and the dynamic evolution of their dispersal centres is critical to understanding how ice sheets evolve and how they shape glacial landscapes. Both empirical and numerical reconstructions can help predict how current ice sheet melting may influence global temperatures, how global temperatures might affect melting rates, and their influence on global sea levels (Napieralski *et al.*, 2007; Löfverström *et al.*, 2014). However, large uncertainties remain concerning the configuration, subglacial regimes, and ice flow chronology of large portions of the Laurentide Ice Sheet (LIS), especially in remote regions of northern Canada (e.g. Margold *et al.*, 2018).

The Quebec–Labrador Dome (QLD), a major ice dispersal centre in the eastern sector of the Laurentide Ice Sheet, persisted throughout the last glacial cycle (Dyke, 2004) and covered an area of about 3 000 000 km^2. At the last glacial maximum (LGM), the QLD was up to 2.5 km thick (Fig. 1A) and likely had several dynamic saddles or secondary ice divides extending across north-central Quebec and northwest Labrador (Dyke and Prest, 1987; Vincent, 1989; Veillette *et al.*, 1999; Dyke, 2004; Parent *et al.*, 2004) including the Labrador Divide. Reconstructing such a large feature of the LIS has been a challenging task, especially due to the complexity of ice flow directional indicators across the region. As a result, the location, migration, and subglacial regime of the QLD have long been debated and are still uncertain (Hughes, 1964; Klassen and Thompson, 1993; Clark *et al.*, 2000; Jansson *et al.*, 2002). The retreat of the ice margin has been constrained by glacial lake reconstructions (Clark *et al.*, 2000), ^{10}Be cosmogenic ages (Carlson *et al.*, 2007; Ullman *et al.*, 2016; Dubé-Loubert *et al.*, 2018), and widely spaced radiocarbon minimum-limiting ages which are largely restricted to coastal regions (compiled by Dyke *et al.*, 2004). The ice margin retreat is known to have occurred rapidly (Ullman *et al.*, 2016); however, the configuration of ice margin retreat is poorly confined within the interior Quebec region (Fig. 1B). Our understanding of the style, timing, and rate of ice margin retreat for this core region would improve with an increased density of chronological constraints.

The goals of this study are to characterize the surficial geology, determine the local ice flow chronology, gain insights into subglacial dynamics, and constrain the timing of deglaciation for the region north of the Quebec–Newfoundland and Labrador provincial border, an area that experienced a complex, yet unresolved ice flow history (Fig. 2). This investigation included surficial mapping based on aerial photographs coupled with ground truthing and outcrop-scale ice flow measurements to determine local ice flow chronologies, which were then integrated into the broader regional context. To constrain the timing of deglaciation within the region, ^{10}Be exposure age dating was applied to bedrock and perched erratics and optical dating methods were applied to glaciolacustrine beach sediments and proglacial outwash sands to constrain the local timing of ice margin retreat.

*Correspondence: J. M. Rice, as above.
E-mail: j4rice@uwaterloo.ca

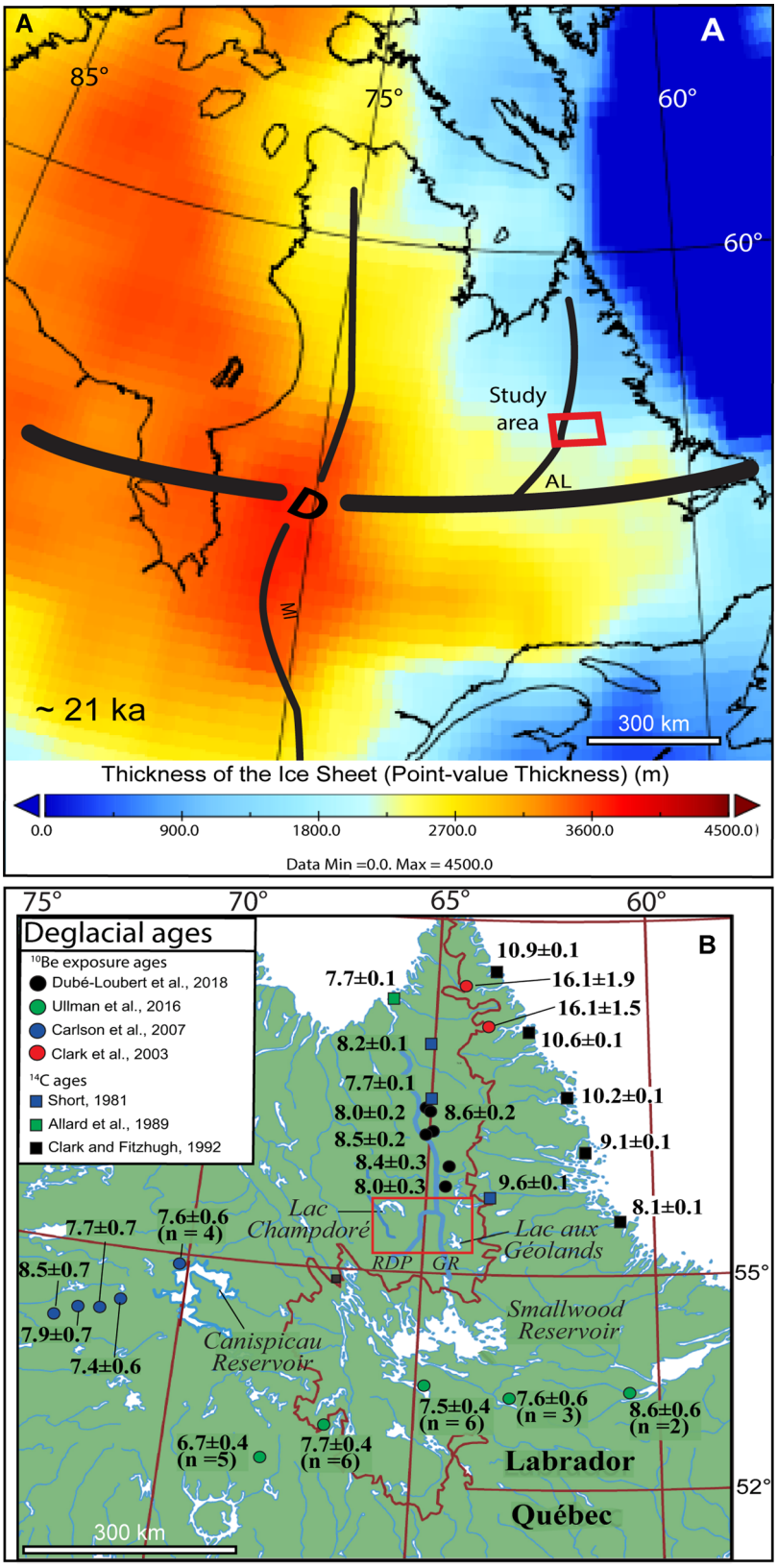

Figure 1. **(A)** Location of the study area within the context of the Laurentide Ice Sheet with ice thickness as modelled by ICE-6G (VM5a) dataset (Argus *et al.*, 2014; Peltier *et al.*, 2015) with major ice dome (QLD) and regional ice divides Mistassini (MI) Ancestral Labrador Ice divide (a.k.a. Labrador Divide) (AL) annotated on top (Dyke and Prest, 1987). **(B)** Study area with major geographical locations identified and previously reported deglacial ages (^{14}C ages are reported in cal a BP and ^{10}Be ages have been calculated using the Baffin Bay production rate of Young *et al.* (2013)). RDP is the *Rivière De Pas* and GR is the George River. [Color figure can be viewed at wileyonlinelibrary.com]

The patterns of glacial sediment distribution, in conjunction with ice flow indicators, and deglacial ages, have allowed for a robust local reconstruction that contributes to an understanding of how the LIS operated in one of its core regions. The constraints on ice flow chronology will also be useful for future ice sheet reconstructions.

Previous work

Striation measurements that suggested a dispersal centre shifted from east of James Bay to northwest of the modern-day Caniapiscau Reservoir were first reported by Low (1896). One of the first regional ice flow chronologies was created through aerial photo landform mapping and ice flow

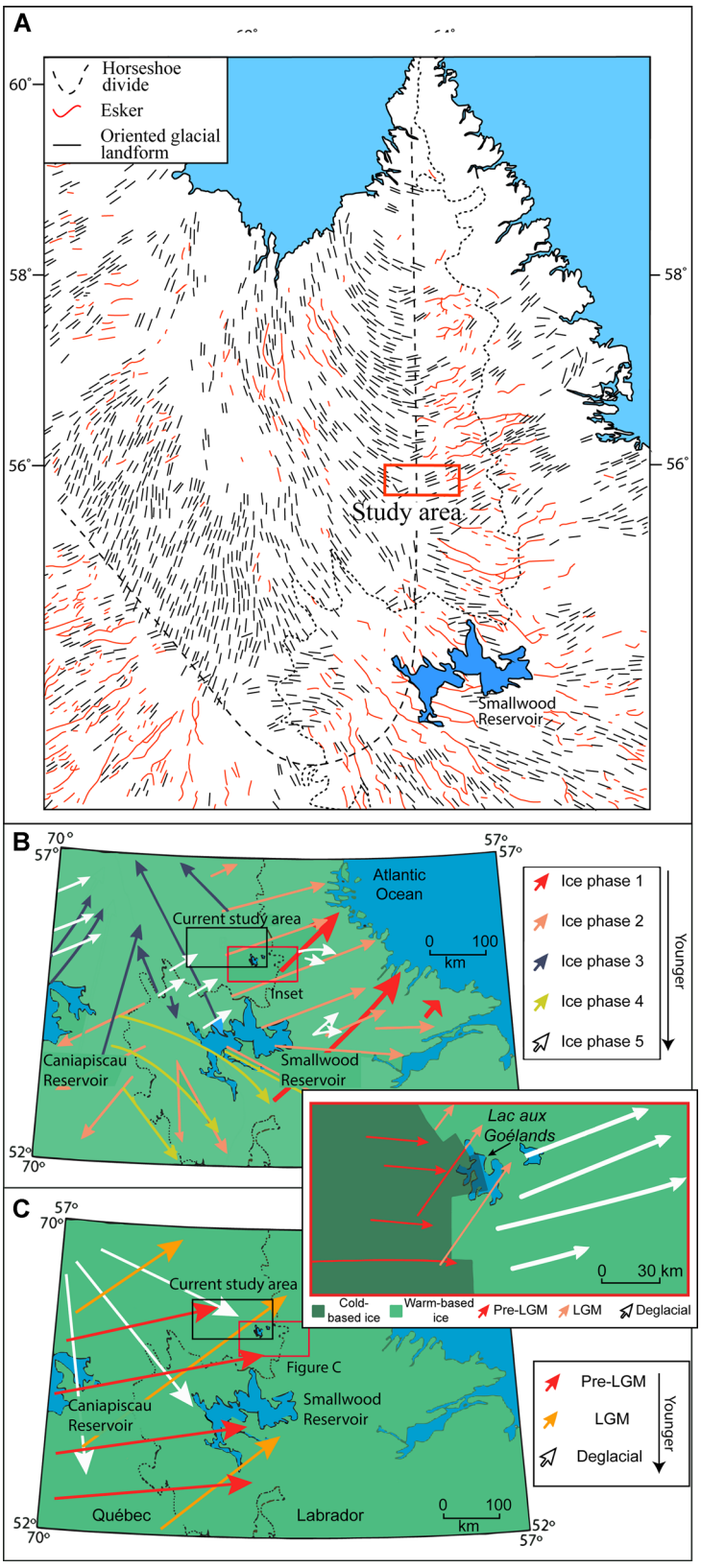

Figure 2. **(A)** Regional distribution and orientation of eskers and glacial landforms across Quebec and Labrador. The dotted line represents the horseshoe divide marking the transition from landforms converging toward Ungava Bay to landforms radiating away from Ungava Bay. Landforms have been redrawn from Fulton (1995). **(B)** Regional ice flow reconstruction by Klassen and Thompson (1993) and Veillette *et al.* (1999) showing five phases of ice flow. Our study area is outlined in black, and *Inset* location is also outlined in red. **(Inset)** Contrasting ice flow reconstruction by Clarhäll and Jansson (2003) indicating that the oldest flow of Klassen and Thompson (1993) and Veillette *et al.* (1999) (Fig. 2B, ice phase 1, red arrow) was a late-Wisconsin ice flow phase (Fig. 2C, LGM flow, orange arrow). Consequently, their ice flow three (Fig. 2B, purple arrow) was actually a deglacial divergent flow away from Ungava Bay (Fig. 2C, white arrow). **(C)** Regional ice flow of Clarhäll and Jansson (2003) and Jansson *et al.* (2002). [Color figure can be viewed at wileyonlinelibrary.com]

measurements by Henderson (1959), indicating an old flow to the south-southwest followed by a northeasterly flow, followed by topographically controlled flows to the northwest, north and southeast. This complex ice flow history was used as evidence by Ives (1960a) to suggest that the region had been the location of an ice dispersal centre. Hughes (1964) conducted systematic mapping of landforms and striations around the Labrador Trough and indicated that the ice divide was located somewhere on the Labrador Trough as erratics from the trough were observed more than 100 km west of their source. Hughes (1964) also recognized a boundary between glaciofluvial landforms and glacial landforms converging northward into Ungava Bay and radially oriented landforms southward away from Ungava Bay (Fig. 2A), subsequently referred to as the horseshoe unconformity (Clark *et al.*, 2000; Jansson *et al.*, 2002; Jansson *et al.*, 2003; Dubé-Loubert and Roy, 2017). More extensive landform mapping, striation measurements, and erratic dispersal train analysis in western

Labrador have brought additional evidence largely consistent with Hughes' (1964) ice flow chronology (Fig. 2B; Klassen and Thompson, 1987, 1993; Klassen and Paradis, 1990).

Chronological striation-based reconstruction by Veillette *et al.* (1999) around the Caniapiscau Reservoir aligned with the earlier work by Hughes (1964) and Klassen and Thompson (1993) with the oldest northeastward-trending flow having a large geographical extent and having originated somewhere in the highlands north of the St Lawrence River (Fig. 2B). Veillette *et al.* (1999) also concluded that the Ungava Bay swarm was the youngest subglacial bed in the region, having formed during the onset of deglaciation around 10 ka.

Clark *et al.* (2000) identified multiple ice streams within the Ungava Bay 'landform swarm', indicating a much more complex glacial history associated with the converging landforms. Through this work, Clark *et al.* (2000) were unable to establish an age relationship between Klassen and Thompson (1993) and Veillette *et al.* (1999)'s Flow II and Flow III. Nonetheless, they were able to conclude that the ice margin retreat was rapid along the southern margin but slower along the northern margin. In addition, they interpreted a shift in ice sheet thermal regime from cold-centred to entirely cold-based associated with ice sheet thinning before it fragmented into smaller ice caps. The complex landforms identified by Clark *et al.* (2000) were further analyzed by Jansson *et al.* (2003) who interpreted the 'Ungava Bay Landform Swarm' (UBLS) as the imprint of the dynamic Ungava Bay Ice Streams (UBIS) that formed during deglaciation.

Southeast of the Ungava swarm in the Lac aux Goélands (Whitegull Lake) region (Fig. 2 inset), Clarhäll and Jansson (2003) documented eastward-trending ice flow indicators within a zone they interpreted as having been preserved under cold-based conditions. In their reconstruction, the ice divide migrated north and occupied the region south of the UBLS, preserving relict glacial landscapes in that area (Fig. 2C). They also attributed the landforms in the region to brief events within otherwise long periods of cold-based conditions until final deglaciation (Fig. 2, inset). In summary, they attribute the landforms in the Lac aux Goélands area to brief events interspersed between long periods of cold-based conditions until final deglaciation.

Deglaciation has been constrained by proglacial lake features (Clark *et al.*, 2000; Dubé-Loubert and Roy, 2017). The timing of deglaciation in the region is based on several ages (Fig. 1B) from the Torngat Mountains to the George River (Clark *et al.*, 2003; Marquette *et al.*, 2004; Staiger *et al.*, 2005; Carlson *et al.*, 2008; Ullman *et al.*, 2016; Dubé-Loubert *et al.*, 2018). Work by Clark *et al.* (2003), Carlson *et al.* (2008) and Ullman *et al.* (2015, 2016) showed evidence that the region west of the Caniapiscau Reservoir was ice free by 8.2 ± 0.5 ka and the region to the south of the Smallwood Reservoir deglaciated later at 6.7 ± 0.4 ka. This led to the conclusion that the ice margin in that sector of the LIS retreated rapidly. North of 56° N, within the George River Basin Dubé-Loubert *et al.* (2018) analyzed and dated shorelines and outburst-flood related landforms and concluded that glacial Lake Naskaupi drained catastrophically at 8.3 ± 0.3 ka. Glacial Lake Naskaupi and glacial Lake McLean were two proglacial lakes that formed during the ice margin retreat within our study area (Ives, 1960a, 1960b; Dubé-Loubert and Roy, 2017). The pathway and timing of the drainage of Lake Naskaupi have been well-defined (Dubé-Loubert and Roy, 2017; Dubé-Loubert *et al.*, 2018); however, its southern extent has not been verified through field investigation. There are also no age constraints on Lake McLean and its extent has been defined only through aerial photo investigation (Ives, 1960b). Finally, there is a large spatial gap between the geochronological transects in the regions, including this study area (Fig. 1B).

Methodology

Surficial mapping

For this work, two 1:100 000 scale surficial geology maps (Rice *et al.*, 2017a, 2017b) were composed using black and white aerial photographs (1:60 000 scale). The photographs provide a stereoscopic three-dimensional visualization of the landscape which enhances the accuracy of surficial unit separation based on vegetation, topography, reflectivity and texture of the surface (Mollard and James, 1984). Field verification of mapped surficial units was completed during three summer field seasons. A total of 142 sites were investigated to validate mapped surficial units.

Relative ice flow chronology

Ice flow directions were first determined using oriented glacial landforms (e.g. crag-and-tail forms, drumlins, and large-scale glacial lineations) identified through both aerial photo and satellite imagery interpretation. Landsat 8 satellite image mosaics were coupled with digital elevation models (DEM) from Canadian Digital Elevation Data (www.geobase.ca 30 m vertical and horizontal resolution) following procedures outlined by Clark *et al.* (2000) and Stokes and Clark (2001). These landform features often form flowsets that cross-cut each other allowing for the development of relative age chronology at the landscape scale (e.g. Kleman and Stroeven, 1997; Clark *et al.*, 2000). However, flowsets do not always clearly overlap and some ice flow phases are not always preserved at the landscape scale. Remote sensing analysis was supplemented with a total of 94 outcrop-scale ice flow indicator measurements, including striations, grooves, rat tails, and mini-*roches moutonnées* (*cf.* McMartin and Paulen, 2009). Following the methodology of Klassen and Bolduc (1984), Parent *et al.* (1995), Veillette and Roy (1995), Veillette *et al.* (1999) and Paulen *et al.* (2013) the ice flow chronology was determined through lee-side preservation, where ice flow indicators on the lee-side position are assumed to indicate earlier (older) ice flow events. The azimuths of the striae and grooves were determined from outcrop shape and lee-side plucking features (Rea *et al.*, 2000). The relative chronology established from outcrop-scale indicator analysis is then compared with the surrounding landform record to establish a more relative age chronology of all observed multiscale ice flow indicators. We thus follow several other researchers (e.g. Parent *et al.*, 1995; Veillette *et al.*, 1999; McMartin and Henderson, 2004; Trommelen *et al.*, 2012; Gauthier *et al.*, 2019) in adopting an approach whereby the pattern and orientation of subglacial streamlined landforms are correlated to the different ice flow directions identified in outcrop striation measurements. Furthermore, because glacial land systems are typically fragmented near core regions of ice sheets (*cf.* Gauthier *et al.*, 2019), patterns of ice flow indicators (both landform flowsets and outcrop-scale records) are also analyzed across the study area to determine whether disjointed zones with internally coherent records can be identified. This is an important step in the identification and characterization of different palimpsest glacial beds (e.g. Kleman and Glasser, 2007). In this conceptual model, unmodified older subglacial land systems are preserved due to a shift from warm-based active ice to cold-based, non-erosive ice. Typically, these relict unmodified terrains are identified next to an area where they are variably overprinted by younger ice flow events.

The evolution of ice sheet dynamics can thus be deciphered, to an extent, in a large study area based on all the above concepts and methods. There are inherent uncertainties associated with these types of landscape analyses and an ice

sheet reconstruction is always incomplete and fragmentary due to the erosion of older flows by younger flows and the resultant incomplete preservation of the full record at any location. Nonetheless, it provides useful insights into the long-term behaviour of ice sheets and is critical to understanding glacial landscapes and their evolution.

Geochronological constraints

Previously reported deglacial ages from the surrounding region (Carlson *et al.*, 2007, 2008; Ullman *et al.*, 2016; Dubé-Loubert *et al.*, 2018) are used in conjunction with deglacial chronology developed as part of this study.

Cosmogenic ^{10}Be exposure dating

Glacially eroded, well-polished, bedrock and perched glacial erratics have proven to be good targets for determining cosmogenic ^{10}Be exposure ages, hereafter simply '^{10}Be ages' (see Appendix S1 for detailed methodology). For our study, eight locations were selected from which to collect bedrock samples for ^{10}Be chronology. At each site, a single bedrock sample was collected from the highest windswept bedrock outcrops with high quartz content. At two of the bedrock sites (15-PTA-081E and 15-PTA-077E), erratic boulders were also sampled. Boulders were selected based on quartz content (quartz > 35%), size (> 1 m^3), stability (no evidence of post-depositional movement), and absence of topographic shielding. Samples were collected along an east–west transect, perpendicular to the regional ice margin retreat direction of Dyke and Prest (1987) to capture the timing of deglaciation across the study area. Ages were calculated using the online exposure age calculator v.3 (http://hess.ess.Washington.edu) using the Baffin Bay/Arctic ^{10}production rate (Young *et al.*, 2013) and the nuclide- and time-dependent scaling scheme (Lifton *et al.*, 2014). We treat all ^{10}Be results as 'apparent ages' due to the potentially added uncertainty caused by cosmogenic nuclide inheritance (see Appendix S1). A detailed description of cosmogenic ^{10}Be exposure sample sites are shown in the Supplementary Material (Fig. S1) and detailed dating methods can also be found in the Supplementary Material (Appendix S1; Table S1). Field and laboratory chemistry data are presented in Table 1.

Optical dating

Optically stimulated luminescence (OSL), hereafter referred to as 'optical dating' has been used successfully to date the formation of glaciolacustrine beaches (e.g. Lepper *et al.*, 2013; Hickin *et al.*, 2015). The utility of this method depends on sampling littoral facies with depositional settings that exposed feldspar grains to sufficient sunlight prior to final burial. Therefore, to further constrain the timing of deglaciation, coarse-to-fine-grained sandy-beach sediments associated with the two identified glacial lakes were targeted for optical dating as they contain sand-sized particles that were more likely to have experienced complete resetting prior to burial (Fuchs and Owen, 2008). Samples were collected by digging vertically into the sediments, taking note of the stratigraphy, to access sediment suitable for optical dating. Elevation data for each site were collected with a hand-held GPS. Samples were collected following the procedures outlined by Aitken (1998) and Lian (2013). A total of four samples were collected for optical dating. Three ages were determined from the analysis of coarse-to-fine-grained littoral sediments and a third age was calculated from fine-grained subaqueous outwash sediments. Samples 15-PTA-035 (elev: 464 ± 5 m) and 15-PTA-149 (elev: 486 ± 5 m) (Figs. 3,4) are from the littoral sediments of Lake Naskaupi in the northeastern section of the study area. Sample 16-PTA-052 (elev: 426 ± 5 m) was collected from a coarse-to-medium-grained sand facies associated with littoral sediments of Lake McLean on an upland peninsula in the northwest region of the study area (Fig. 3). Sample 15-PTA-074 (elev: 314 ± 5 m) was collected from a fine-grained, subaqueous, outwash fan deposited into Lake Naskaupi likely near its lowest level in the region, providing an age for the late stages of Lake Naskaupi. Glaciofluvial outwash sediments have a lower bleaching probability (Fuchs and Owen, 2008); however, they have been used successfully in other studies (*cf.* Klasen *et al.*, 2006; Alexanderson and Murray, 2007; Bøe *et al.*, 2007). Samples were submitted to the Luminescence Dating Laboratory at the University of the Fraser Valley, Abbotsford, British Columbia, where optical dating analysis was conducted on sand-sized K-feldspar grains, as the optical signal from quartz was found to be unsuitable because it lacked the desired so-called 'fast component' (Bailey *et al.*, 1997). Experimental procedures specific to this study can be found in the Supplementary Material (Appendix S2). Detailed sample site figures are shown in the Supplementary Material (Fig. S2). Field and laboratory data are described in Table 2.

Results

Bedrock and till landscapes

The highlands are characterized by bedrock outcrops draped by a discontinuous thin till veneer (Fig. 5A), often with large perched erratics and thicker deposits of till in the lower relief areas which mask the underlying bedrock topography. Bedrock outcrops are also observed where glaciofluvial outwash or proglacial lake wave erosion has removed the glacial sediments (Fig. 6). Streamlined landforms occur in the east of the study area (Fig. 7), with steep stoss and gradual lee-side slopes characteristic of drumlins (a-axes up to 3 km long) and more elongated smaller glacial lineations with less steep stoss edges (a-axes 1.5 km long) oriented to the northeast. Large drumlins (a-axes 4 km long) oriented to the northwest are also observed, but in lower quantities in the most northwestern portion of the study area. Till of varying thickness is the most abundant surficial sediment across the study area (Fig. 6). There were no exposures showing glacial stratigraphy within the study area.

Meltwater features

Glaciofluvial deposits are common within the central portions of the map sheet, where subglacial drainage channels are abundant (Fig. 5B). These channels are typically incised into the glacial sediments but are also found as V-shaped channels eroded into bedrock up to 8 m deep. The smaller channels usually lead to larger meltwater systems that eventually drain to the east and west of the central upland. In the eastern portion of the study area, these meltwater channels transition into depositional systems, forming large sinusoidal eskers fanning eastward toward the Labrador coast. The generally parallel (~10–12 km between eskers) eastward organization of the eskers indicates a local drainage pattern oriented east-southeast associated with meltwater drainage during deglaciation. These eskers are associated with the large radial pattern of eskers in the region correlated with the retreat of the QLD ice margin toward central Quebec (Occhietti *et al.*, 2004, 2011). These large esker systems are oblique to subglacial lineations in the region, which is a key observation indicating that the northeasterly ice flow indicators in

Table 1. ^{10}Be sample information for bedrock and erratic (E) samples.

Sample	Latitude (°N)	Longitude (°W)	Elev. (masl)	Corr. Elev. (masl)a	Thick (cm)	Topo. shielding correction	[Be-10] atoms/g	± atoms /g	Exposure age (LSDn ± 1 σ (yrs))b	1 σ (%)
EAST										
16-PTA-058	55.843	-64.207	494	433	3.0	1	1.23E + 03	1.23E + 03	7800 ± 200	2.6%
15-PTA-078	55.821	-64.515	517	456	2.5	1	6.28E + 04	1.24E + 03	9800 + 200	2.0%
15PTA-081†	55.810	-64.189	559	498	2.0	1	6.10E + 04	2.03E + 04	9200 + 3100	33.7%
15PTA-081E†	55.810	-64.189	559	498	1.5	1	4.13E + 04	1.37E + 04	6200 + 2100	33.9%
CENTRE										
15PTA-077†	55.810	-65.080	495	434	3.0	1	4.35E + 04	1.78E + 04	7100 + 2900	40.8%
15PTA-077E†	55.810	-65.080	495	434	2.0	1	1.03E + 05	2.35E + 04	16700 + 3800c	22.8%
16-PTA-070	55.784	-65.251	623	562	1.0	1	1.67E + 05	3.14E + 03	24000 + 500c	2.1%
WEST										
16-PTA-053	55.867	-65.709	517	456	3.0	1	5.36E + 04	1.19E + 03	8500 + 200	2.4%
15-PTA-083	55.772	-65.721	509	448	1.0	1	5.95E + 04	1.14E + 03	9500 + 200	2.1%
15PTA-021†	55.838	-65.729	529	468	2.0	1	5.07E + 04	1.14E + 04	7900 + 1800	22.8%

[a]Elevations were corrected to isostatic uplift by averaging the uplift from modern elevation using data from ICE-6G(VM5a) (Argus *et al.* 2014; Peltier *et al.*, 2015).
[b]Error is reported to 1σ of internal uncertainty. Values have been rounded to nearest 10 s value.
[c]Outlier samples
[†]Sample analyzed by PRIME lab.

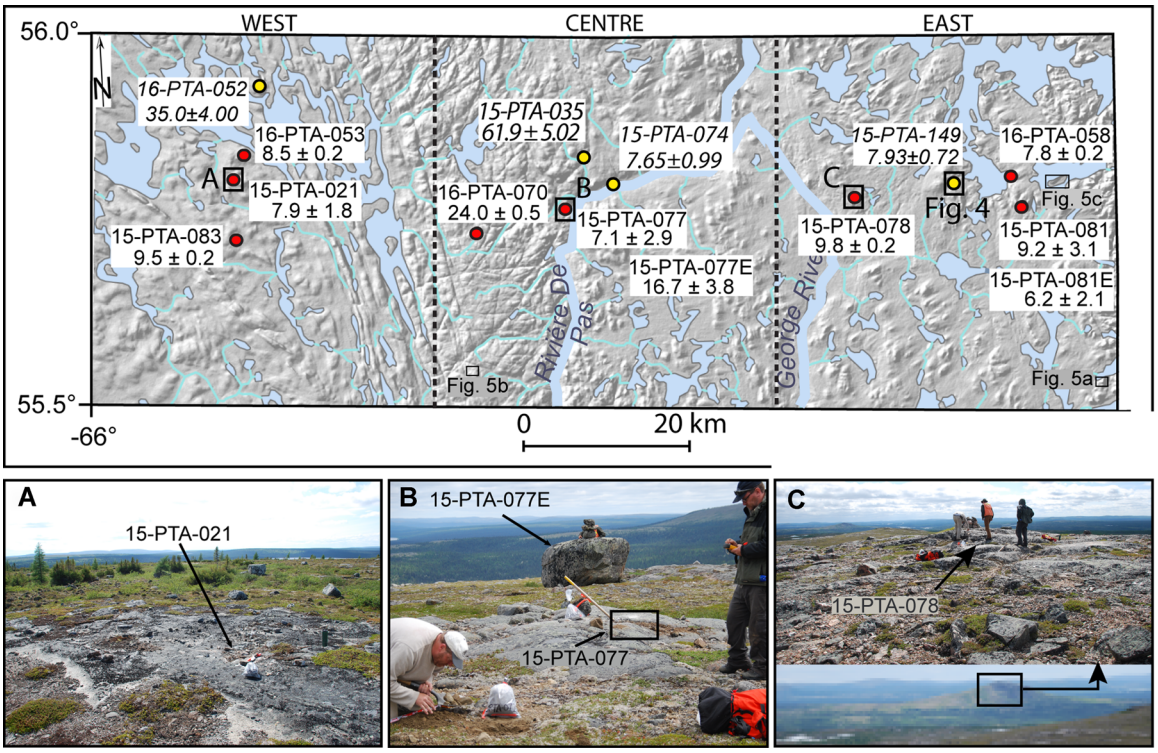

Figure 3. Sample location of ^{10}Be cosmogenic exposure samples (red) and OSL samples (yellow) with calculated ages. Ages are reported in thousands of years before present (ka). **(A)** Sample site 15-PTA-021 from the western portion of the map sheet. The sample was collected from exposed bedrock on an upland clearing. **(B)** Sample site 15-PTA-077 (foreground) and 15-PTA-077E (background) collected from an exposed bedrock outcrop and perched erratic on a windswept upland near the *Rivière De Pas*. **(C)** Sample 15-PTA-078 collected from bedrock outcrop (top image) located on the knob of a large crag-and-tail (bottom image). [Color figure can be viewed at wileyonlinelibrary.com]

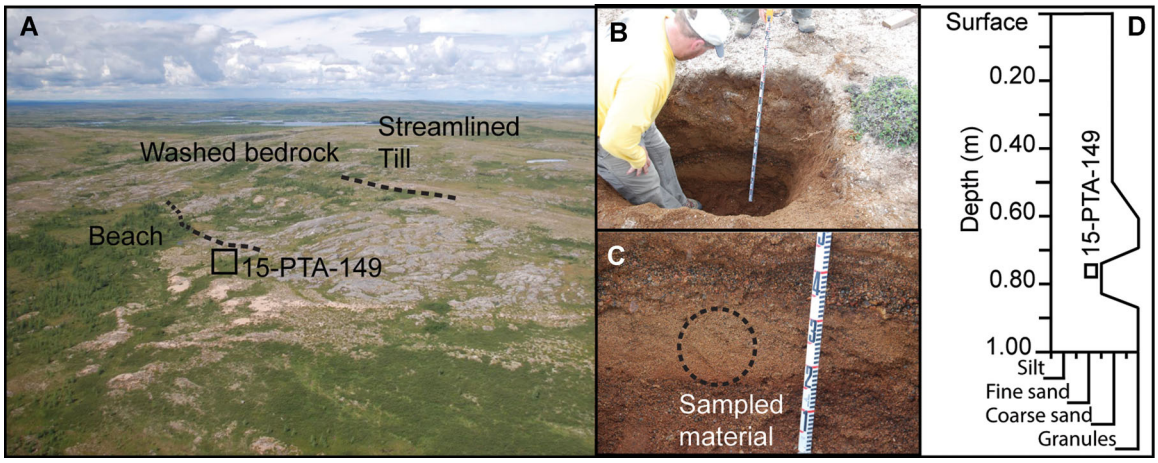

Figure 4. Optical dating sample 15-PTA-149 collected from littoral sediments below the washing limit of glacial Lake Naskaupi (elev. 486 ± 5 m a.s.l.). [Color figure can be viewed at wileyonlinelibrary.com]

the study area (see below) predate the establishment of the channelized draining system that deposited the eskers.

Glaciolacustrine features

The two glacial lakes that inundated the study area, Naskaupi and McLean, occupied the general basins of present-day *Lac Mistinibi* in the east and *Lac Champdoré/Lac Tudor* in the west, respectively (Fig. 6 purple). Although no fine-grained, ice-distal, glacial-lake deposits were identified within the study area, well-developed beach ridges associated with each lake were mapped (Fig. 5C). Our fieldwork confirms that Lake McLean extended south of 56° N and the highest elevation inundated at 426 m a.s.l. (± 5 m) with a second level of well-developed beaches approximately 15 m lower in elevation. In the eastern portion of the study area, multiple beach ridges associated with Lake Naskaupi were identified. The maximum elevation of Lake Naskaupi within the study area was 486 ± 5 m a.s.l., with well-developed lower shorelines at 462 ± 5 m a.s.l.

Ice flow indicators and relative chronology

A total of 306 glacial streamlined landforms have been mapped in the study area (Fig. 7). They consist of rock and till drumlins, *roches moutonées* and small streamlined till ridges. They are concentrated in three zones across the study area: (1) northeastward-trending landforms in the northeast (n = 165, average azimuth = 70°); (2) northwestward-trending landforms in the northwest (n = 60, average azimuth = 288°); and (3) eastward-trending landforms on the eastern flank of the central highlands (n = 81, average azimuth = 87°). Only a few (n = 3) cross-cutting landforms were identified within the study area,

Table 2. Optically stimulated luminescence sample collection data.

Sample ID	Elev. (± 5 masl)	Depth (cm)	H_2O (Δ^w)†	K (%)	Rb (ppm)	Th (ppm)	U (ppm)	D_e (CAM) (Gy)	Uncorrected CAM age (ka)	Fading- corrected CAM‡ age estimate (ka)§	Fading- corrected MAM‡ age estimate (ka)§
15-PTA-035	464	100	0.0088 ± 0.001	2.50 ± 0.13	52.5 ± 2.77	3.00 ± 2.77	0.39 ± 0.08	23.0 ± 4.0	40.0 ± 3.2	61.9 ± 5.02	29.9 ± 3.10
15-PTA-074	314	370	0.185 ± 0.002	1.80 ± 0.1	61.8 ± 3.31	5.50 ± 0.28	2.13 ± 1.69	7.0 ± 1.0	6.13 ± 0.79	7.65 ± 0.99	n/a
15-PTA-149	486	75	0.0329 ± 0.003	2.40 ± 0.1	108 ± 5.50	5.50 ± 0.28	1.30 ± 0.11	33.0 ± 5.0	6.59 ± 0.60	7.93 ± 0.72	4.59 ± 0.45
16-PTA-052	426	140	0.021 ± 0.010	2.9 ± 0.1	80 ± 5.0	20.6 ± 0.5	1.3 ± 0.1	120.8 ± 10.8	21.6 ± 3.6	35.0 ± 4.0	15.5 ± 2.7 (20.5 ± 3.5)

†Water contents are 'as collected' values and are defined as (mass water)/(mass minerals).
‡Fading corrections were applied using the method of Huntley and Lamothe (2001). Because the natural signal (Ln/Tn) falls in the non-linear part of the dose–response curves of samples (Fig. 8), this correction method may underestimate the true age by~15–20% (*cf.* Mathews *et al.*, 2015).
§MAM ages in brackets excludes two lowest outlying D_e values (Fig. 8).

with large Flow 1 landforms cross-cut by small Flow 3 landforms. Striations were also observed and analyzed at 94 sites across the study area (Supplementary data Table S2). At 41 of these sites, multiple ice flow phases were identified (Fig. 7). The striation sites with multiple phases of ice flow were critical in developing a relative ice flow chronology, which was used to establish which singular striations sites were associated with which ice flow phase. Most striations and grooves preserved in the lee side of numerous outcrops sculpted by later flows indicate ice flow toward the northeast (Fig. 8). Notably, the majority of these observations were made at sites located in the eastern portion of the study area where a number of streamlined landforms trending in the same general direction were also mapped (Fig. 7). Based on this, sites with northeastward-trending indicators across the study area were correlated to Flow 1 (Fig. 8). A total of 76 sites with striations and grooves were associated with the oldest ice flow to the northeast. The orientation of these outcrop-scale ice flow indicators range in direction from 20 to 90° with a mean azimuth of 55° ($\sigma^1 = 12.5°$).

The second phase of ice flow (Flow 2) was identified from outcrop-scale microforms measured at 19 sites across the study area (Fig. 8). These ice flow measurements were constrained to the western portion of the study area (Fig. 8). Microforms measured in the study area indicated a west-northwesterly ice flow ranging in direction between 286 and 332° with a mean azimuth of 305° ($\sigma^1 = 10.4°$). Three sites were critical in establishing this flow as being younger than Flow 1 (Figs. 7,8).

At 12 key sites, features associated with older flows (Flows 1 and 2) are cross-cut by younger eastward-trending ice flow indicators (Fig. 7) and three landforms associated with Flow 3 have slightly reworked older, larger landforms from Flow 1. Additionally, the eskers mapped in the study area also trend eastward. Based on these relationships, all the eastward-trending ice flow features are correlated to the third phase of ice flow (Flow 3, Fig. 8). Outcrop-scale ice flow measurements associated with Flow 3 indicate a southeast-to-eastward flow ranging in direction between 52 and 140° with a mean azimuth of 83° ($\sigma^1 = 16.1°$).

Finally, ice flow features indicating flow to the west-southwest, ranging between 229 and 270° with a mean azimuth of 248° ($\sigma^1 = 14.1°$) have also been observed at 13 sites. These ice flow indicators were the youngest flow at each site where they were identified (Fig. 8). These ice flow measurements were restricted to the central and western portions of the study area. They are correlated to our youngest ice flow phase (Flow 4, Fig. 8).

Deglacial chronology

^{10}Be ages

^{10}Be ages are summarized in Fig. 3, with detailed site information in the supplementary data (Fig. S3). Samples were grouped according to their spatial proximity (eastern group, central group, and western group, Fig. 3). Summed probabilities were created for each group using ^{10}Be ages to evaluate the approximate timing of deglaciation for each group (Fig. 9). The ^{10}Be ages in the eastern group (n = 4) range from 6.2 ± 2.1 to 9.8 ± 0.2 ka. The central group (n = 3) had the largest variance in ^{10}Be ages, ranging from 7.1 ± 2.9 to 24.0 ± 0.5 ka (Fig. 9). The western group (n = 3) reveals the tightest clustering of ages ranging from 7.9 ± 1.8 to 9.5 ± 0.2 ka (Fig. 9). We consider two ^{10}Be ages of 24.0 ± 0.5 ka (16-PTA-070) and 16.7 ± 3.8 ka (15-PTA-077E), which are significantly older than the others, to be outliers. These two samples, one from bedrock (16-PTA-070) and the other from an erratic

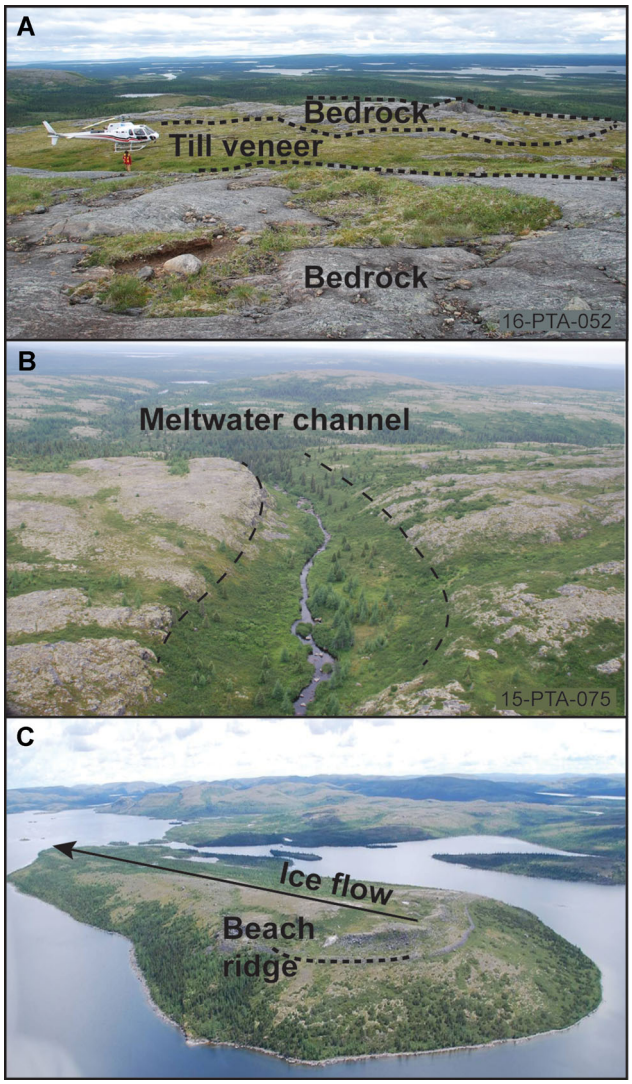

Figure 5. Location of features are indicated on Figure 3. **(A)** An example of bedrock uplands with a thin till veneer and thicker till blanket in the valley in the background. **(B)** An example of a deep meltwater channel (~ 8 m). **(C)** An example of a large streamlined landform winnowed by glacial Lake Naskaupi, leaving a cobble beach near the top of the landform. [Color figure can be viewed at wileyonlinelibrary.com]

(15-PTA-077E), likely experienced insignificant glacial erosion and thus contain inherited ^{10}Be (Briner *et al.*, 2005). Because of this, samples 16-PTA-070 and 15-PTA-077E have been removed from our deglacial age discussion and figures.

Optical dating

Two samples, 15-PTA-149 (elev. 486 ± 5 m) and 15-PTA-035 (450 ± 5 m) were collected for optical dating from proglacial littoral sediments associated with Lake Naskaupi. They yielded ages of 7.93 ± 0.72 and 61.9 ka ± 5.02 ka BP, respectively (Fig. 10; Table 2). A third sample, 15-PTA-074 (314 ± 5 m), was collected from an outwash fan deposit associated with Lake Naskaupi. These outwash sediments formed during the late stages of the proglacial lake and yielded an age of 7.65 ± 0.99 ka BP (Fig. 10; Table 2). Data from the only sample collected from Lake McLean (16-PTA-052) indicate a minimum age of 35.5 ± 4.0 ka. Given what is known about the regional deglacial history, this result, and that from sample 15-PTA-035 are clearly anomalous. It is likely that these age values result from poor bleaching prior to deposition, which can be common in advanced-phase glacial outwash environments that are typically turbid (Fuchs and Owen, 2008), or that were deposited as an outwash delta into the lake (see Supplementary Material for more details). Because of this, we have omitted these two samples from the discussion of our deglacial ages. Laboratory results from the optical dating experiments are reported in the Supplementary Material (Appendix S2, Fig. S3 and Tables S3, S4 and S5).

Interpretation and discussion

Ice-flow reconstruction

Flow 1: The earliest ice flow indicators identified in the study area provide evidence of ice flow to the northeast. Evidence for this oldest northeastern ice flow event is found across the central and eastern portions of the study area (Fig. 8). This ice flow event was also reported in recent surficial maps to the south (Paulen *et al.*, 2017; Campbell *et al.*, 2018), indicating that the ice sheet flowed in a generally uniform northeasterly pattern across the study area with only slight deviations, as

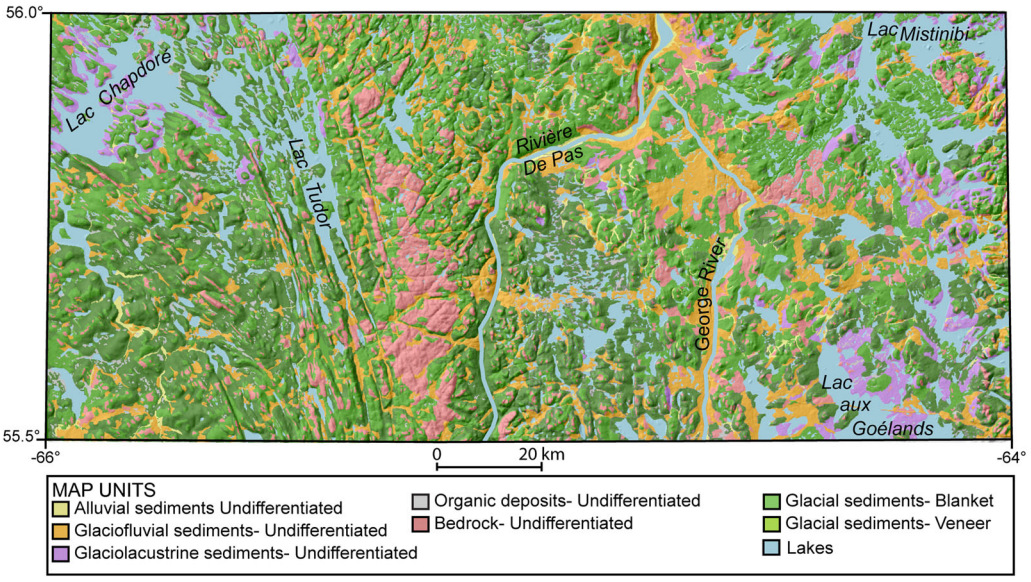

Figure 6. A simplified surficial map compiled from two 1:100 000 surficial geology maps (Rice *et al.* 2017a, 2017b). The large north-to-south trending bedrock outcrop (red) in the centre of the map is the *De Pas* Batholith. Surficial deposits have been draped over a 30 m resolution Shuttle Radar Topography Mission imagery derived hillshade (www.earthexplorer.usgs.gov). [Color figure can be viewed at wileyonlinelibrary.com]

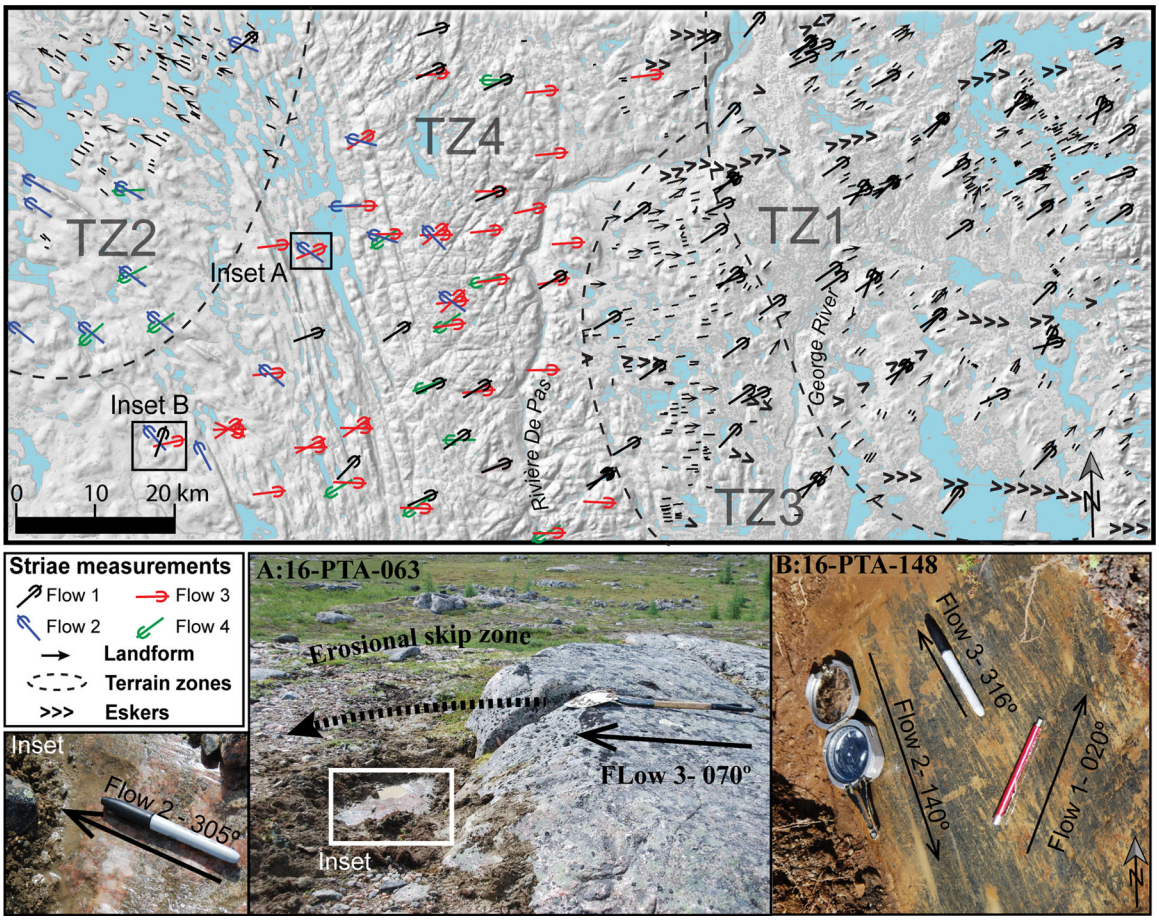

Figure 7. Hillshade DEM of the study area with outcrop-scale ice flow indicators and mapped oriented glacial landforms. **(A)** Sample site 16-PTA-063 gives an example of the lee-side protection of Flow 2 from Flow 3, indicating that Flow 2 is younger in age. **(Inset)** closer view of Flow 2 in lee-side protected surface. **(B)** Three phases of ice flow exemplified by deep grooves associated with the oldest ice flow, with finer and more abundant striations from later ice flow phases (sample 16-PTA-148). [Color figure can be viewed at wileyonlinelibrary.com]

recorded in striae azimuths (Fig. 8). Our investigation extends Klassen and Thompson's (1993) E1 ice flow phase (Fig. 2B, red arrow) further northwest than previously reported. However, it is lacking in the northwestern part of the study area and it is not known whether this is due to local cold-based conditions during Flow 1, or if the records of this flow were eroded during subsequent ice flow phases (e.g. Flow 2).

An abundance of large glacially scoured landforms was also identified in the northeastern portion of the study area, parallel to striation measurements associated with Flow 1 and are presumed to have been created during the same ice flow event (Fig. 8). Altogether, these observations suggest that Flow 1 was an erosive flow that was sustained for a considerable period (Clark, 1993). In addition, the degree of preservation of old northeastward-trending features in the eastern portion of the study area and lack of overprinting by younger features, suggest a shift from warm-based to cold-based subglacial conditions in the eastern portion of the study area (Figs. 7,8). Only the eskers seem to cross-cut the features associated with Flow 1 in that area. Notably, orientations of the eskers to the east-southeast differ from the landforms and striations associated with Flow 1 by~50°, which indicates that Flow 1 must have occurred prior to the formation of the eskers, at a time when the ice sheet had a different configuration. These northeastward-trending landforms were not included in Clark *et al*'s. (2000) reconstruction of the QLD, but are presumed to predate their flowsets (or group of similarly oriented landforms) 19 to 23, as landforms within our study area with similar orientation to Clark *et al.* (2000)'s flowset 19 formed during a later ice flow event (see below).

Flow 1 represents a large-scale glacial flow from an ice mass somewhere to the south-southwest likely centred in the Quebec Highlands (Klassen and Thompson, 1993; Veillette *et al.*, 1999; Parent *et al.*, 2004). The timing of this ice flow event, how long this flow was sustained, its possible duration, or if there were any earlier glacial events, is currently unclear. Veillette *et al.* (1999) reported outcrops striated by a north-easterly flow with a ferromanganese varnish, which was considered to be evidence of long exposure to weathering from an interglacial period (striated bedrock surfaces do not typically show this kind of weathering in northern Canada). Additionally, Klassen *et al.* (1988) reported inter-till stratified units at a single site in the Labrador Trough, indicating an ice flow event followed by an ice-free period. However, no evidence of ferromanganese staining or inter-till (non-glacial) units was observed in this study area. In addition, three bedrock outcrops in the eastern portion of the study area, where the northeast-trending flowset is dominant, yielded apparent ^{10}Be ages that are considered close to the deglacial age (Fig. 3) suggesting that the amount of inheritance (little to no inheritance) over this landscape is not indicative of a relict glacial landscape from pre-Wisconsin glaciation (Briner *et al.*, 2006). Nonetheless, a more detailed investigation would be required in order to more completely test the pre-Wisconsin interpretation of that flowset, including an analysis of weathering across the flowset area. Therefore, it is likely that Flow 1 is the oldest preserved flow phase in the study area, and it likely occurred at a time of extensive and thick ice due to the overall record of a uniform regional flow. Our findings related to Flow 1 corroborate Klassen and Thompson's (1993) and

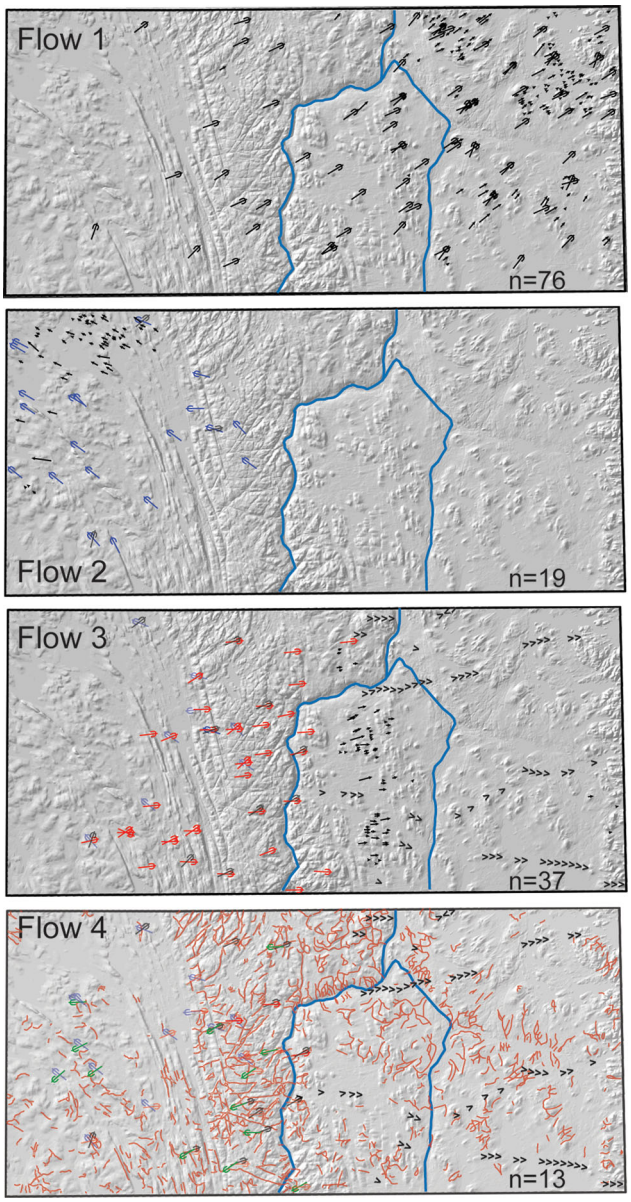

Figure 8. Ice flow diagrams with supporting striae and landforms. Where multiple ice flow phases were recorded at one site, the ice flow indicators from previous flow were left on younger ice flow figures to aid in interpreting the relative ages for each flow: **(Flow 1)** the oldest ice flow phase in the study area to the northeast as identified by landforms and striations. **(Flow 2)** The second phase of ice flow to the northwest as identified by striations and landforms. **(Flow 3)** The third phase of ice flow, following a westward migration of the ice divide, characterized by flow to the east as evident from striations and landforms. Eskers (») have been included on this diagram to indicate that the ice margin retreated from the east-southeast to the north-northwest at least until the *Rivière De Pas*. **(Flow 4)** The final phase of ice flow is associated with a late-deglaciation flow of an independent ice cap, with local ice flow largely resulting from the local topography. Evidence of this flow is only observed in the striation record. Meltwater channels (red) have also been overlain. [Color figure can be viewed at wileyonlinelibrary.com]

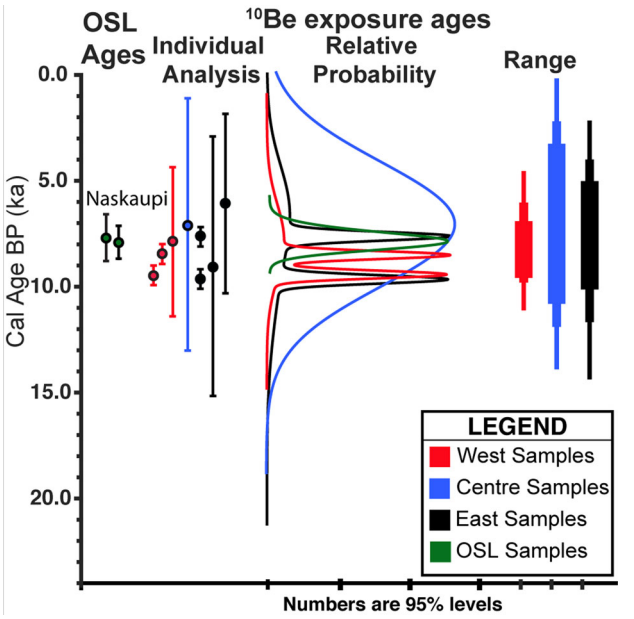

Figure 9. Plot showing the individual calculation of each ^{10}Be exposure age and optical age sample, the relative probability of the age for each group of samples, and the range of ages for each group (east (black), centre (blue), west (red), and glacial lakes (green)). The ages included on the matchstick figures (Range) indicate the 5th percentile, the peak probability of the sample, and the 95th percentiles of the samples. Note: ^{10}Be exposure samples 16-PTA-070 and 15-PTA-077E and optical ages 15-PTA-035 and 16-PTA-052 not included in this figure (see Results). [Color figure can be viewed at wileyonlinelibrary.com]

Veillette *et al.*'s (1999) earliest flow phase (Fig. 2B, red arrow) and add new evidence which now extends this flow's influence further north into the study area.

Flow 2: Following Flow 1, an ice flow switch is recorded in the western half of the study area. Flow 2 represents flow toward the northwest that was initiated somewhere over the highlands in the central portion of the study area (Fig. 8). The age relationship between these two flows was established from outcrop-scale ice flow indicators from Flow 1 that are cross-cut or preserved in the lee side of outcrop sculpted by Flow 2 at three locations (Fig. 8). The landforms in the northwestern portion of the study area also trend to the northwest (Fig. 8). The abundance of streamlined bedrock landforms in the western region suggests a highly erosive flow. This may explain the lack of older features within that flowset.

Klassen and Thompson (1993) reported ice flow indicators of similar orientation to Flow 2, which they associated with the swarm of landforms toward Ungava Bay, but associated them with their third flow phase (Fig. 2B, purple arrow). We also correlate our Flow 2 to the Clark *et al.* (2000) Flowset 19 and Jansson *et al.* (2003) Fan D. These flowsets were suggested to have formed during deglaciation. In their reconstruction of the Ungava Ice Stream, Jansson *et al.* (2003) suggested that Fan D was a relatively early phase in the evolution of the ice stream catchment. Our findings suggest Flow 2 features also formed at a relatively early stage of deglaciation as they are locally overprinted by younger phases. We can therefore constrain this flow as having occurred at some time before the formation of Flow 3 features and associated eastward-trending eskers. Based on the reconstruction of the Ungava Ice Stream by Jansson *et al.* (2003), Flow 2 would have shut down and the catchment would have moved further west. One possible scenario is that this evolution led to a progressive shift of the ice divide toward the west over the Flow 2 flowset. This shift would have preserved Flow 2 under the ice divide and started forming Flow 3 features to the east.

Flow 3: Outcrop-scale ice flow indicators from Flow 2 are cross-cut or preserved in the lee side of outcrop sculpted by Flow 3 at seven key locations (Fig. 8). As indicated above, this shift suggests the dispersal centre migrated westward, across the study area, likely influenced by the UBIS (Clark *et al.*, 2000; Jansson *et al.*, 2003). This change in dynamics caused ice to flow eastward (Flow 3), possibly pulled by ice streams to the east (ice stream #187, Margold *et al.*, 2018) although Flow 3 appears to be restricted to the central portion of the study area and could thus have developed later; coeval to the eskers.

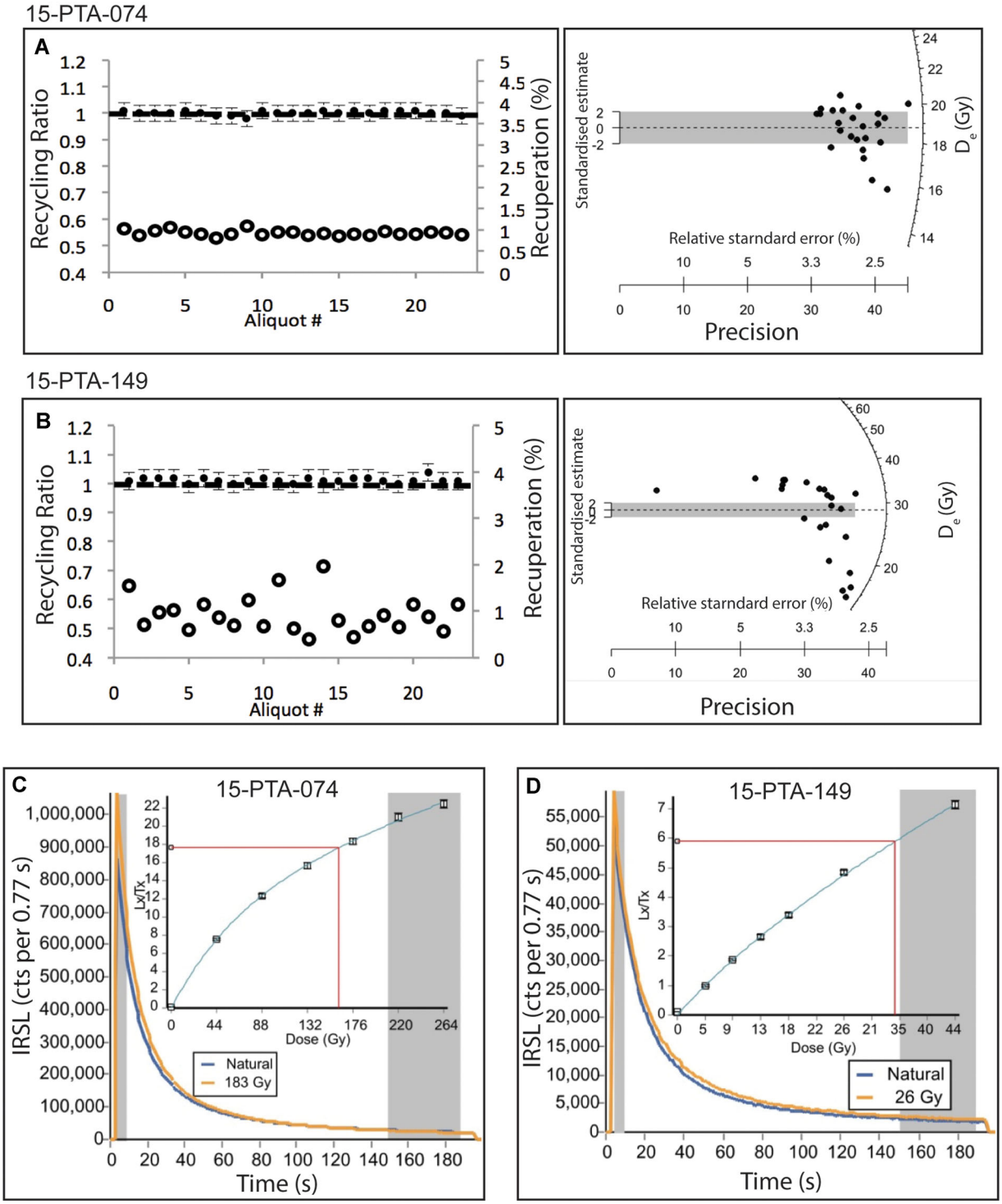

Figure 10. Recuperation values, recycling ratios, and D_e distributions for samples 15-PTA-074 **(A)** and 15-PTA-149 **(B)**. The shaded region on the decay curves marks the initial and final parts of the optical signal used to calculate the equivalent dose (D_e) value. Optical decay curves and dose–response curves (inset) for optical samples 15-PTA-0174 **(C)** and 15-PTA-149 **(D)**. See Supplementary data for graphs from all collected samples. [Color figure can be viewed at wileyonlinelibrary.com]

As these landforms could not have formed directly under the ice divide, it is unlikely that the landforms of Flow 2 and Flow 3 formed isochronously and therefore likely formed time-transgressively, as the ice divide migrated westward across the study area. However, it is possible that Flow 2 and Flow 3 operated coevally for some time during ice divide migration. These two flows were likely separated by the eastern arm of the horseshoe divide that was being influenced by the changing dynamics of surrounding ice streams; however, more detailed work would be required to confirm this. The preservation of ice flow indicators from Flow 1 and Flow 2 in the western portion of the study area (Fig. 7) suggest that subglacial conditions in that part of the study area shifted to a cold-based thermal regime during Flow 3, preserving the older ice flow indicators. Furthermore, the erosive intensity of the ice sheet was minimal within the central highlands of the study area, as evident from the lack of glacially sculpted landforms in this region, and from cross-cutting, opposing, striations associated with numerous double stoss-and-lee outcrops (Fig. 11). Additionally, the landforms associated with Flow 3 have the same general orientation of elongate eskers in the eastern part of the study area (Fig. 8) and were likely formed at the late

stages of Flow 3 when the ice bed conditions switched to warm-based as eskers typically form during late-stage meltwater flow (Shilts *et al.*, 1987; Boulton *et al.*, 2009).

Klassen and Thompson's (1993) deglacial ice flow (Fig. 2A, phase 2, orange arrows) and Clarhäll and Jansson's (2003) deglacial phase (Fig. 2, white arrow) all have a similar orientation to our deglacial Flow 3. Landforms from this flow were not identified by Clark *et al.* (2000). Dubé-Loubert and Roy (2017) reported a similar pattern of eskers that shows a general retreat from east to west which stops at the George River valley area, ~135 km north of our study area. These eskers transition to frost-shattered bedrock and oxidized glacial deposits with multiple instances of lateral meltwater channels east of the George River associated with sustained cold-based conditions. Dubé-Loubert and Roy (2017) indicated the ice retreat was irregular and fragmented caused by changes in the basal thermal regime of the melting ice sheet. Our findings lend additional support to this reconstruction, although evidence of sustained cold-based conditions, such as felsenmeer or other types of weathered *in situ* regolith is lacking in the study area. It is possible that the ice divide in our study area was more sensitive and responded more to changes taking place in Ungava Bay than the area located to the north where Dubé-Loubert and Roy (2017) completed their work.

Flow 4: Following Flow 3 there was late-deglacial flow (Flow 4) to the east-southeast (Fig. 8). Flow 4 overprints striations of all previous flows and was identified at 13 locations. There are no landforms associated with this ice flow phase, suggesting it was likely short-lived and not highly erosive (Stokes and Clark, 2001), most likely due to thinner ice. This ice flow event was not identified by Clarhäll and Jansson (2003) but was identified by Klassen and Thompson (1993) and Veillette *et al.* (1999) and was associated with both reconstructions' divergent phase 2 (Fig. 2, orange arrow). Our striation evidence firmly constrains Flow 4 to have occurred after Flow 3 and the formation of elongated eskers. It is still unclear as to how the ice margin and overall retreat of the LIS evolved from Flow 3 to Flow 4.

Ives (1958) and Kirby (1961) reported multiple sets of lateral meltwater channels and discordant striation measurements that indicated small ice caps in the Schefferville and Kivivic Lake regions. These findings support the scenario of multiple retreating ice centres proposed by Clark *et al.* (2000), whereby small ice caps formed during deglaciation, turned cold-based, and retreated toward the central highlands. Therefore, either the ice thinned to a point at which the bedrock topography became the predominant control on ice flow direction (Flow 4), and/or similar to other observations in the region (Ives, 1958; Clark *et al.*, 2000), a small ice cap formed somewhere on the De Pas upland before the final disappearance of the ice mass.

Timing of deglaciation

Following a deglacial flow to the east (Flow 3), the ice sheet began to significantly melt, and meltwater flowed to the central upland cutting large meltwater channels. These channels fed meltwater drainage systems toward the east which deposited large eastward-trending eskers. At some point following the formation of the eskers, proglacial Lake Naskaupi formed in the upper George River valley (Dubé-Loubert and Roy, 2017) and, presumably, Lake McLean formed in the general basin of modern-day *Lac Champdoré*. During deglaciation, a late stage, short-lived ice cap developed on the central upland (Flow 4), followed by final melting under cold-based conditions which formed abundant lateral meltwater channels (Fig. 8).

The ^{10}Be results lack a clear separation in ages between the eastern, central, and western groups. The large spread in ages within the central spatial group (Fig. 9, blue) is indicative of inheritance within the samples. This inheritance is presumably the result of glacial erosion insufficient to remove all previous accumulations of ^{10}Be (Fabel *et al.*, 2004; Briner *et al.*, 2005). This supports our ice flow reconstruction model where sluggish, less erosive ice occupied the central portions of the map sheet with limited subglacial erosion throughout ice divide migration. A more detailed investigation of the cosmogenic inheritance across the landscape and of related glacial erosion would significantly improve a discussion on the changing subglacial conditions across the region.

^{10}Be ages from perched erratics to the south and west of this study by Carlson *et al.* (2007; 2008) indicated that the LIS began retreating rapidly from the Hudson Bay coast at 8.2 ka and the entire region was completely ice free by 6.8 ± 0.2 ka. Additionally, Ullman *et al.* (2016) suggested that the dominant loss of ice from the LIS occurred by 7.6 ± 0.6 ka following a rapid retreat of ice margins. Our optical and ^{10}Be results range from 9.8 to 6.2 ka (Fig. 9; Table 1). This relatively broad range is mostly due to the uncertainty of some of the ^{10}Be ages. The two OSL results that were considered reliable cluster within a slightly narrower range of 7.7–7.9 ka. These results are consistent with Ullman *et al.*'s (2016) reconstruction, considering the distance between the two study areas and the general deglaciation pattern. Our results also correlate reasonably well with the more local ^{10}Be ages from the Lake Naskaupi shoreline, which indicate that Lake Naskaupi must have reached its largest extent before draining catastrophically at 8.3 ± 0.3 ka (Dubé-Loubert *et al.*, 2018). This event is further confined by the optical dating of Lake Naskaupi highest (sample 15-PTA-149; 7.93 ± 1.0) and lowest (sample 15-PTA-074; 7.65 ± 1.0) levels in the study area (Fig. 3), which matches Dubé-Loubert *et al.*'s (2018) findings well. Unfortunately, samples from Lake McLean yielded no usable results, therefore a discussion on its formation and drainage is not possible without further investigation.

Palaeoglaciological implications

Records indicating ice flow reversals have been documented elsewhere and interpreted as evidence of ice divide migration; most notably, within the Keewatin ice divide region (McMartin and Henderson, 2004) and in the Canadian Arctic (Dyke *et al.*, 1992) but also just west of our study area (Parent *et al.*, 2004). In this study, the ice flow shift between Flow 1 and Flow 2 may not necessarily require ice divide migration, as it may have been caused by the development of the UBIS. However, the degree of preservation of Flow 1 features to the east suggest that an ice divide developed over that zone separating the UBIS from the ice flow dynamics further to the east toward the Labrador coast. Furthermore, an ice divide migration appears to best explain both the preservation of Flow 2 in the northwest and the development of Flow 3 features to the east. This type of ice divide migration is not of the same magnitude as the one documented in the Keewatin (~500 km: McMartin and Henderson, 2004) and does not require a large ice sheet reorganization. Nonetheless, it influenced the study area's landscape evolution and it shows the impact that an ice stream catchment zone can have on the glacial dynamics far inland (e.g. Ross *et al.*, 2009; Rignot *et al.*, 2011).

It appears that subglacial conditions also evolved from regionally widespread warm-based conditions during Flow 1 to a polythermal base, which led to the preservation of Flow 1 features in the eastern portion, partial overprinting in the central portion by subsequent flows, and more intense

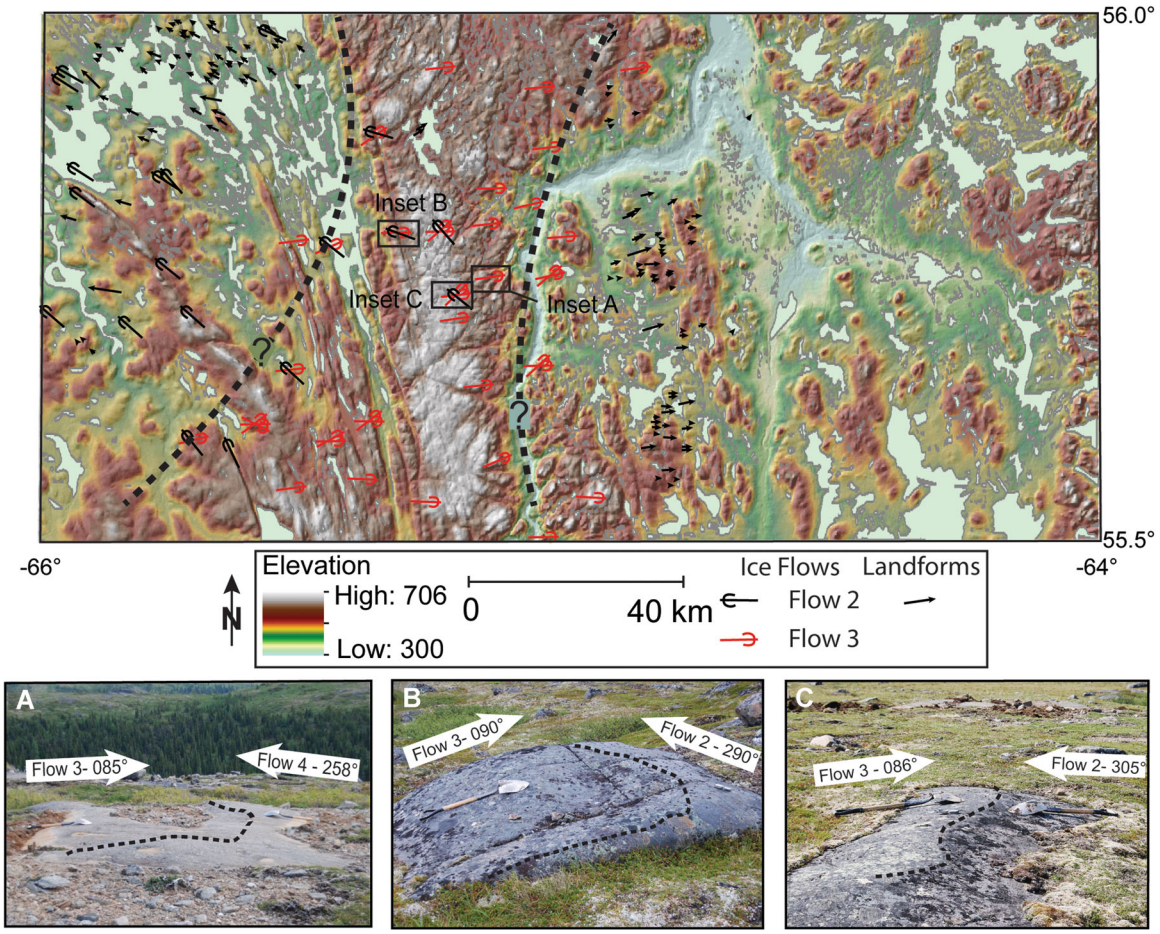

Figure 11. Hillshaded and elevation classed regional DEM with striations from ice flow phase 2 (black) and phase 3 (red). The region of substrate protection is highlighted with dashed lines. The *De Pas* Batholith is evident as the elevated ridge (white colour on the DEM) bisecting the map sheet just west of the *Rivière De Pas*. **(A)** Outcrop from sample site 15-PTA-024 with evidence of ice flow reversal. **(B)** Bevelled outcrop at sample site 15-PTA-058 formed by two near opposing ice flow directions. **(C)** Double stoss-and-lee outcrop at sample site 16-PTA-069 again created by two near opposing ice flow phases. [Color figure can be viewed at wileyonlinelibrary.com]

overprinting during Flow 2 in the northwest. The net effect of this evolution is a mosaic terrain at the landscape scale somewhat similar to the fragmented landscape described in the outer zone of the Keewatin (Trommelen *et al.*, 2012; Gauthier *et al.*, 2019). This is best shown in the landform record, where Flow 1, Flow 2 and Flow 3 are limited to their own spatial zones, with only minor cross-cutting of the flows evident in the striation record (Fig. 8). Long intervals in which the base of the ice is near or below the pressure melting point (limited net erosion) are needed to generate the landscape fragments or zones containing multiple ice flow indicators of highly variable directions.

These two ice domes (Keewatin and Labrador) were the largest and probably thickest mid-latitude ice sheet domes of the last glaciation (e.g. Dyke and Prest, 1987; Tarasov *et al.*, 2012). These ice domes have left a unique record that contrasts with other ice divide areas. For example, smaller and thinner ice domes over Baffin Island (Davis *et al.*, 2006), the Boothia and Melville peninsulas (De Angelis and Kleman, 2005), and in central Sweden (Kleman and Stroeven, 1997), have widespread evidence of sustained cold-based conditions and lack evidence for major ice divide translocation. These other smaller ice divides at higher latitudes appear to have remained relatively stationary throughout glaciation. The LIS thus had polythermal ice divide regions that migrated throughout glaciation, preserving ice flow mosaics from different ice flow directions. This complex mosaic is recognizable at multiple scales, not just at the large landform-scale (*cf.* Boulton and Clark, 1990), such as within the regional striation record and by small-scale landforms. Here we argue that this approach, where landform mapping is supplemented with outcrop-scale observations, is key in the reconstruction of ice flow dynamics and resolution of existing and conflicting ice flow reconstructions. The multiple sites where different ice flow events are recorded in the striation record were critical in resolving the ice flow history of the study area, for which conflicting ice flow reconstructions existed. Additional research on glacial erosion and till transport, and further investigation into cosmogenic radionuclide inheritance in both bedrock and till (e.g. Staiger *et al.*, 2006), should help further test and improve these reconstructions and add to our overall understanding of ice sheet and landscape evolution in ice divide regions.

Conclusions

The purpose of this research was to constrain the relative ice flow chronology in a debated region that had insufficient field observations and to establish the local timing of deglaciation. This work builds on regional glacial reconstructions conducted nearby which were intended to elucidate the complex ice flow chronology through extensive field-based investigations. We have resolved the conflicting ice flow chronologies (*cf.* Veillette *et al.*, 1999; Jansson *et al.*, 2002) within the study

area, with four ice flow phases identified from striae measurements and landform analysis. The first ice flow phase was uniform to the northeast across most of the study area, which was followed by the propagation of the UBIS within the western portion of the study area, which dispersed ice to the northwest and formed large oriented landforms. A change in subglacial thermal regime took place in the eastern portion which favoured the preservation of Flow 1 features. Flow 3 marks an important shift toward the deglaciation of the region, as the UBIS influence became weaker in the study area. Ice then stagnated or was sluggish in most areas, eskers developed, and the ice margin retreated from the east to the west toward the George River. A short-lived late-deglacial phase from the central highlands to the west-southwest occurred during deglaciation as recorded by weak and discontinuous late-stage ice flow indicators (Flow 4). The exact timing of these ice flow events remains unknown. Optical ages from Lake Naskaupi indicate that beach ridges associated with the lake were formed around 7.9 ± 0.7 ka and this is consistent with the detailed deglacial work conducted by Dubé-Loubert *et al.* (2018) north of our study area, which provides additional constraints south of their study area to constrain the timing of local deglaciation.

Future work on confining the subglacial conditions across the region should help to further elucidate the complex evolution of the QLD throughout glaciation, providing important constraining parameters for future ice sheet scale reconstructions (e.g. Clark *et al.*, 2000; Dyke *et al.*, 2004; Margold *et al.*, 2018).

Supporting information

Additional supporting information may be found in the online version of this article at the publisher's web-site.

Appendix S1. Detailed methodology for ^{10}Be exposure dating.

Appendix S2. Detailed methodology for optical dating.

Figure S1. Sample locations and site photos for ^{10}Be samples 16-PTA-053, 15-PTA-083, 16-PTA-070, 16-PTA-058, 15-PTA-081 and 15-PTA-081E.

Figure S2. Sample locations and site photos for optical dating samples 15-PTA-074, 15-PTA-035 and 16-PTA-052.

Figure S3. Recuperation values, recycling ratios, D_e distributions, optical decay curves, and dose–response curves for OSL samples.

Table S1. Isostatic rebound correction calculations for cosmogenic ^{10}Be age determination. **Table S2.** Summary of striation data collected from within the study area.

Table S3. Dosimetry information for optical age samples 15-PTA-035, 15-PTA-074, 15-PTA-149 and 16-PTA-052.

Table S4. SAR protocol used for OSL samples.

Table S5. Sample dose equivalent (D_e) values and ages for optical age samples 15-PTA-035, 15-PTA-074, 15-PTA-149 and 16-PTA-052.

Acknowledgements. This research was funded by the Geological Survey of Canada's Geo-Mapping for Energy and Minerals II (GEM2) Program (2013–2020) with support from the Polar Continental Support Program under the Core Zone Surficial Activity (Hudson–Ungava Project) and a Research Affiliate Bursary to the first author. Generous funding was also provided by the Northern Scientific Training Program (NSTP) and the Ontario Graduate Scholarship (OGS) fund to the first author. The authors thank Matt Pyne (GSC, Ottawa) Grant Hagedorn, Hugo Dubé-Loubert, and Alan Lion for their enthusiastic field assistance. Avriel Schweinsberg prepared samples in the University at Buffalo Cosmogenic Isotope Laboratory. Travis Gingerich (University of the Fraser Valley) prepared the optical dating samples and assisted with measurements. Research at the Luminescence Dating Laboratory at the University of the Fraser Valley was supported by a Natural Science and Engineering Research Council (NSERC) of Canada Discovery Grant and an NSERC Research Tools and Instruments Grant to Olav B. Lian. Tom Lowell is thanked for the Matlab script used in producing summed probability diagrams. Michel Parent (GSC Quebec) is thanked for his constructive comments on an earlier version of this manuscript. Reviewers 1 and 2 are also thanked for their thoughtful reviews. (NRCan Contribution number: 20180338).

References

Aitken MJ. 1998. *An Introduction to Optical dating*. Oxford University Press: Oxford; 267.

Alexanderson H, Murray AS. 2007. Was southern Sweden ice free at 19-25 ka, or were the post LGM glaciofluvial sediments incompletely bleached? *Quaternary Geochronology* **2**: 229–236.

Argus DF, Peltier WR, Drummond R, *et al.* 2014. The Antarctica component of postglacial rebound model ICE- 6G_C (VM5a) based upon GPS positioning, exposure age dating of ice thicknesses, and relative sea level histories. *Geophysics Journal International* **198**: 537–563.

Bailey RM, Smith BW, Rhodes EJ. 1997. Partial bleaching and the decay form characteristics of quartz OSL. *Radiation Measurements* **27**: 123–136.

Bøe A-G, Murray A, Dahl SO. 2007. Resetting of sediments mobilized by the LGM ice-sheet in southern Norway. *Quaternary Geochronology* **2**: 1–4.

Boulton GS, Clark CD. 1990. A highly mobile Laurentide ice sheet revealed by satellite images of glacial lineations. *Nature* **346**: 813–817.

Boulton GS, Hagdorn M, Mailot PB, *et al.* 2009. Drainage beneath ice sheets: groundwater-channel coupling, and the origin of esker systems from former ice sheets. *Quaternary Science Reviews* **28**: 621–638.

Briner JP, Kaufman DS, Manley WF, *et al.* 2005. Cosmogenic exposure dating of late Pleistocene moraine stabilization in Alaska. *Geological Society of America Bulletin* **117**: 1108–1120.

Briner JP, Miller GH, Davis PT, *et al.* 2006. Cosmogenic radionuclides from fiord landscapes support differential erosion by overriding ice sheets. *Geological Society of America Bulletin* **118**: 406–420.

Campbell HE, Paulen RC, Rice JM 2018. Surficial geology, Ashuanipi River, Newfoundland and Labrador, NTS 23-I southwest. *Geological Survey of Canada, Canadian Geoscience Map* 346. Scale 1:100 000.

Carlson AE, Clark PU, Raisbeck GM, *et al.* 2007. Rapid Holocene deglaciation of the Labrador sector of the Laurentide Ice Sheet. *Journal of Climate* **20**: 5126–5133.

Carlson AE, LeGrande AN, Oppo DW, *et al.* 2008. Rapid early Holocene deglaciation of the Laurentide Ice Sheet. *Nature Geoscience* **1**: 620–624.

Clarhäll A, Jansson KN. 2003. Time perspectives on glacial landscape formation-glacial flow chronology at Lac aux Goélands, northeastern Québec, Canada. *Journal of Quaternary Science* **18**: 441–452.

Clark CD. 1993. Mega-scale glacial lineations and cross-cutting ice-flow landforms. *Earth surface Processes and Landforms* **18**: 1–29.

Clark CD, Knight JK, Gray JT. 2000. Geomorphological reconstruction of the Labrador Sector of the Laurentide Ice sheet. *Quaternary Science Reviews* **19**: 5126–5133.

Clark PU, Brook EJ, Raisbeck GM, *et al.* 2003. Cosmogenic 10Be ages of the Saglek Moraines, Torngat Mountains, Labrador. *Geology* **31**: 617–620.

Davis PT, Briner JP, Coulthard RD, *et al.* 2006. Preservation of Arctic landscapes overridden by cold-based ice sheets. *Quaternary Research* **65**: 156–163.

De Angelis H, Kleman J. 2005. Paleo-ice streams in the norther Keewatin sector of the Laurentide ice sheet. *Annals of Glaciology* **42**: 135–144.

Dubé-Loubert H, Roy M. 2017. Development, evolution and drainage of glacial Lake Naskaupi during the deglaciation of north-central Quebec and Labrador. *Journal of Quaternary Science* **32**: 1121–1137.

Dubé-Loubert H, Roy M, Schaefer JM, *et al.* 2018. ^{10}Be dating of former glacial Lake Naskaupi (Québec-Labrador) and timing of its

discharge during the last deglaciation. *Quaternary Science Reviews* **191**: 31–40.

Dyke AS. 2004. An outline of North American deglaciation with emphasis on central and northern Canada. In *In Quaternary Glaciations –Extent and Chronology, Part II: North America*, Ehlers J, Gibbard PL (eds). Elsevier: Amsterdam; 371–406.

Dyke AS, Prest VK. 1987. Late Wisconsinan and Holocene history of the Laurentide Ice Sheet. *Geographie Physique et Quaternaire* **41**: 237–263.

Dyke AS, Morris TF, Green DEC, *et al.* 1992. Quaternary Geology of Prince of Wales Island, Arctic Canada. *Geological Survey of Canada Memoir* **433**, https://doi.org/10.4095/134058

Dyke AS, Moore A, Robertson L. 2004. Deglaciation of Canada. *Geological Survey of Canada* Open File **1574**. *Thirty-two maps at* **1**. 7 000 000 scale.

Fabel D, Harbor J, Dahms D, *et al.* 2004. Spatial Patterns of Glacial Erosion at a Valley Scale Derived From Terrestrial Cosmogenic ^{10}Be and ^{26}Al Concentrations in Rock. *Annals of the Association of American Geographers* **94**: 241–255.

Fuchs M, Owen LA. 2008. Luminescence dating of glacial and associated sediment: review, recommendations and future directions. *Boreas* **37**: 636–659.

Fulton RJ 1995. Surficial materials of Canada. *Geological Survey of Canada, "A" Series*, Map 1880A. 1: 5 000 000 scale.

Gauthier MS, Hodder TJ, Ross M, *et al.* 2019. The subglacial mosaic of the Laurentide Ice Sheet; a study of the interior region of southwestern Hudson Bay. *Quaternary Science Reviews* **214**: 1–27.

Henderson EP. 1959. A glacial study of central-Labrador Quebec. *Geological Survey of Canada Bulletin* **40**: 1–94.

Hickin AS, Lian OV, Levson VM, *et al.* 2015. Pattern and chronology of glacial Lake Peace Shorelines and implications for isostacy and ice-sheet configuration in northeastern British Columbia, Canada. *Boreas* **44**: 228–304.

Hughes OL. 1964. Surficial geology, Nichicun-Kaniapiscau Map-area. *Geological Survey of Canada Bulletin* **106**: 1–20.

Huntley DJ, Lamothe M. 2001. Ubiquity of anomalous fading in K-feldspars and the measurement and correction for it in optical dating. *Canadian Journal of Earth Sciences* **38**: 1093–1106.

Ives JD. 1958. Glacial Drainage Channels as Indicators of Late-glacial Conditions in Labrador-Ungava: a Discussion. *Cahiers de Geographie de Québec* **3**: 57–72.

Ives JD. 1960a. The deglaciation of Labrador-Ungava- an outline. *Cahiers de Geographie de Québec* **4**: 323–343.

Ives JD. 1960b. Former ice-dammed lakes and the deglaciation of the middle reaches of the George River, Labrador-Ungava. *Geographical Bulletin* **14**: 44–69.

Jansson KN, Kleman J, Marchant DR. 2002. The succession of ice-flow pattern in north central Quebec-Labrador, Canada. *Quaternary Science Review* **21**: 503–523.

Jansson KN, Stroeven AP, Kleman J. 2003. Configuration and timing of Ungava Bay ice streams, Labrador-Ungava, Canada. *Boreas* **32**: 256–262.

Kirby RP. 1961. Movements of ice in Central Labrador-Ungava. *Cahiers de géographie du Québec* **5**: 205–218.

Klasen N, Fiebig M, Preusser F, *et al.* 2006. Luminescence properties of glaciofluvial sediments from the Bavarian Alpine Foreland. *Radiation Measurements* **41**: 866–870.

Klassen RA, Bolduc AM. 1984. Ice flow directions and drift composition, Churchill Falls, Labrador. *Current Research, Geological Survey of Canada Part A* **84-1A**: 255–258.

Klassen RA, Thompson FJ 1987. Ice flow history and glacial dispersal in the Labrador Trough. *In Exploration technology and glacial dispersal studies*, Geological Survey of Canada, Paper no. 87-1A: 61-710.

Klassen RA, Paradis SJ. 1990. Surficial geology, western Labrador (NTS 23 A, B, C, G, I, J and parts of 13 C, 22P, and 23 H). *Geological Survey of Canada Open File* **2198**.

Klassen RA, Thompson FJ. 1993. Glacial history, drift composition, and mineral exploration, central Labrador. *Geological Survey of Canada Bulletin* **435**.

Klassen RA, Matthews JVJ, Mott RJ, *et al.* 1988. The stratigraphic and paleobotanical record of Interglaciation in the Wabush region of western Labrador (abstract). *In Climatic Fluctuations and Man 3, Annual Meeting of the Canadian Committee on Climatic Fluctuations.* Jan. 18-19, Ottawa: 22-26.

Kleman J, Glasser NF. 2007. The subglacial thermal organization (STO) of ice sheets. *Quaternary Science Reviews* **26**: 585–597.

Kleman J, Stroeven AP. 1997. Preglacial surface remnants and Quaternary glacial regimes in northwestern Sweden. *Geomorphology* **19**: 35–54.

Lepper K, Buell AW, Fisher TG, *et al.* 2013. A chronology for glacial Lake Agassiz along Upham's namesake transect. *Quaternary Research* **80**: 88–98.

Lian OB. 2013. Luminescence dating: optical dating. In *Encyclopedia of Quaternary Science*, Elias SA (ed). Elsevier: Amsterdam; 653–666.

Lifton N, Beel C, Hätterstrand C, *et al.* 2014. Constraints on the late Quaternary glacial history of the Inylcheck and Sary-Dzaz valleys from *in situ* cosmogenic ^{10}Be and ^{26}Al, eastern Kyrgyz Tian Shan. *Quaternary Science Reviews* **101**: 77–90.

Low AP 1896. Report on exploration in the Labrador Peninsula along the Eastmain, Koksoak, Hamilton, Manikuagan and portions of other rivers in 1982-93-94-95. *Geological Survey of Canada* Annual Report, 8: Part L.

Löfverström M, Caballero, Nilsson J, *et al.* 2014. Evolution of the large-scale atmospheric circulation in response to changing ice sheets over the last glacial cycle. *Climate of the past* **10**: 1453–1471.

Margold M, Stokes CR, Clark CD. 2018. Reconciling records of ice streaming and ice margin retreat to produce a paleographic reconstruction of the deglaciation of the Laurentide Ice Sheet. *Quaternary Science Reviews* **189**: 1–30.

Marquette GC, Gray JT, Gosse JC, *et al.* 2004. Felsenmeer persistence under non-erosive ice in the Torngat and Kaumajet mountains, Quebec and Labrador, as determined by soil weathering and cosmogenic nuclide exposure dating. *Canadian Journal of Earth Science* **41**: 19–38.

Mathewes RW, Lian OB, Clague JJ, *et al.* 2015. Early Wisconsinan (MIS 4) glaciation on Haida Gwaii, British Columbia, and implications for biological refugia. *Canadian Journal of Earth Science* **52**: 939–951.

McMartin I, Henderson P. 2004. Evidence from Keewatin (Central Nunavut) for paleo-ice divide migration. *Geographie Physique et Quaternaire* **58**: 163–186.

McMartin I, Paulen RC. 2009. Ice-flow indicators and the importance of ice-flow mapping for drift prospecting. In *Application of Till and Stream Sediment Heavy Mineral and Geochemical Methods to Mineral Exploration in Western and Northern Canada*, Paulen RC, McMartin I (eds). Geological Association of Canada, 15–34. GAC Short Course Notes.

Mollard JO, James R. 1984. *Air photo interpretation and the Canadian landscape*. Canadian Government Publishing Centre: Hull, Canada; 415.

Napieralski J, Hubbard A, Li Y, *et al.* 2007. Toward a GIS assessment of numerical ice-sheet model performance using geomorphological data. *Journal of Glaciology* **53**: 71–83.

Occhietti S, Govare É, Klassen R, *et al.* 2004. Late Wisconsinan –Early Holocene deglaciation of Québec-Labrador. In *Quaternary glaciations, Extent and chronology Part II: North America*, Ehlers J, Gibbard PL (eds). Elsevier: New York; 243–273.

Occhietti S, Parent M, Lajeunesse P, *et al.* 2011. Late Pleistocene-Early Holocene Decay of the Laurentide Ice Sheet in Québec-Labrador. *Developments in Quaternary Science* **15**: 601–630.

Parent M, Paradis SJ, Boisvert É. 1995. Ice-flow patterns and glacial transport in the eastern Hudson Bay region: implications for the Late Quaternary dynamics of the Laurentide Ice Sheet. *Canadian Journal of Earth Sciences* **32**: 2057–2070.

Parent M, Beaumier M, Girard R, *et al.* 2004. Diamond exploration in the Archean craton of northern Québec Kimberlite indicator minerals in eskers of the Saindon-Cambrien corridor. *Quebec Ministry of Natural Resources Fauna and Parks*, Manuscript 2004-02.

Paulen RC, McClenaghan MB, Hicken AK. 2013. Regional and local ice-flow history in the vicinity of the Izok Lake Zn-Cu-Pb-Ag deposit, Nunavut. *Canadian Journal of Earth Sciences* **50**: 1209–1222.

Paulen RC, Rice JM, McClenaghan MB. 2017. Surficial geology northwest Smallwood Reservoir, Newfoundland and Labrador NTS

23-I southeast. *Geological Survey of Canada Geoscience Map* **315**. scale: 1: 100 000.

Peltier WR, Argus DF, Drummond R. 2015. Space geodesy constrains ice-age terminal deglaciation: The global ICE-6G_C (VM5a) model. *Journal of Geophysics Research, Solid Earth* **120**: 450–487.

Rea BR, Evans DJA, Dixon TS, *et al.* 2000. Contemporaneous, localized, basal ice-flow variations: implications for bedrock erosion and the origin of p-forms. *Journal of Glaciology* **46**: 470–476.

Rice JM, Paulen RC, Ross M 2017a. Surficial geology, Lac Mistinibi, Quebec, NTS 23-P northeast. *Geological Survey of Canada* Canadian Geoscience Map 316.

Rice JM, Paulen RC, Ross M 2017b. Surficial geology, Rivière De Pas, Quebec, NTS 23-P northwest. *Geological Survey of Canada* Canadian Geoscience Map 333.

Rignot E, Mouginot J, Scheuchl B. 2011. Ice Flow of the Antarctic Ice Sheet. *Science* **333**: 1427–1430.

Ross M, Lajeunesse P, Kosar KGA. 2009. The subglacial record of northern Hudson Bay: insights into the Hudson Straight Ice Stream catchment. *Boreas* **40**: 73-–791.

Shilts WW, Aylsworth JM, Kaszycki CA, *et al.* 1987. Canadian Shield. In *Geomorphic systems in North America*, Graf WL (ed). Geological Society of America, 119–161. centennial Special.

Staiger JKW, Gosse JC, Johnson JV, *et al.* 2005. Quaternary relief generation by polythermal glacier ice. *Earth Surface processes and Landforms* **30**: 1145–1159.

Staiger JW, Gosse J, Little EC, *et al.* 2006. Glacial erosion and sediment dispersion from detrital cosmogenic nuclide analysis of till. *Quaternary Geochronology* **1**: 29–42.

Stokes CR, Clark CD. 2001. Paleo-ice streams. *Quaternary Science Reviews* **20**: 1437–1457.

Tarasov L, Dyke AS, Neal RM, *et al.* 2012. A data-calibrated distribution of deglacial chronologies for the North American ice complex from glaciological modeling. *Earth and Planetary Science Letters* **15**: 30–40.

Trommelen MS, Ross M, Campbell JE. 2012. Glacial terrain zone analysis of a fragmented paleoglacioloic record, southeast Keewatin sector of the Laurentide Ice Sheet. *Quaternary Science Reviews* **40**: 1–20.

Ullman DJ, Carlson AE, Anslow FS, *et al.* 2015. Laurentide ice-sheet instability during the last deglaciation. *Nature Geoscience* **8**: 534–537.

Ullman DJ, Carlson AE, Hostetler SW, *et al.* 2016. Final Laurentide ice-sheet deglaciation and Holocene climate-sea level change. *Quaternary Science Reviews* **152**: 49–59.

Veillette JJ, Roy M 1995. The spectacular cross-striated outcrops of James Bay, Quebec. In *Current Research 1995-C* Geological survey of Canada: 243-248.

Veillette JJ, Dyke AS, Roy M. 1999. Ice-flow evolution of the Labrador Sector of the Laurentide Ice Sheet: a review, with new evidence from northern Quebec. *Quaternary Science Reviews* **18**: 993–1019.

Vincent J-S. 1989. Quaternary geology of the southeastern Canadian Shield. In *Chapter 3 of Quaternary Geology of Canada and Greenland*, Fulton RJ (ed). Geological Survey of Canada, Geology of Canada, no.1.

Young NE, Schaefer JM, Briner JP, *et al.* 2013. A Be-10 production rate calibration for the Arctic. *Journal of Quaternary Science* **28**: 515–526.

